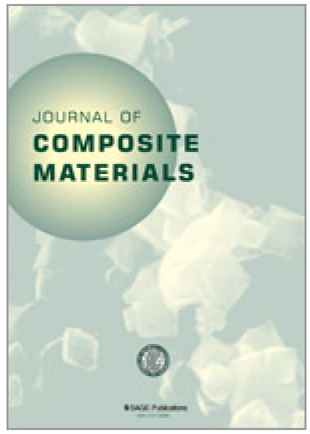

Static analysis of FG plates using T-splines based isogeometric approach and a refined plate theory

Journal:	*Journal of Composite Materials*
Manuscript ID	JCM-20-0734
Manuscript Type:	Original Manuscript
Date Submitted by the Author:	10-Jun-2020
Complete List of Authors:	Liu, Zhenyu; Zhejiang University Wang, Chuang; Zhejiang University Duan, Guifang; Zhejiang University, Tan, Jianrong; Zhejiang University
Keywords:	FG Plates; Static bending; Refined plate theory; T-splines; Isogeometric analysis;
Abstract:	In this study, a novel refined plate theory (RPT) is developed for the static analysis of FG plates, which is a simplification of the higher-order shear deformation theories (HSDTs). It improves the computational efficiency while preserving the accuracy advantage of HSDTs. The C1-continuity problem is overcome by isogeometric analysis (IGA), which shows more advantages than the C0 elements based finite element analysis. By T-splines, the computational costis effectively reduced, since compared to NURBS based IGA, T-splines can achieve local refinement and improve the utilization of control points. The rule of mixture with power-law and Mori–Tanaka scheme are adopted to calculate the material properties of the plate. Several numerical experiments are given to prove the efficiency of the proposed method.

Static analysis of FG plates using T-splines based isogeometric approach and a refined plate theory

Zhenyu Liu, Chuang Wang, Guifang Duan* and Jianrong Tan

The State Key Laboratory of CAD&CG, Zhejiang University, Hangzhou, Zhejiang 310058, China.

* Corresponding Author (e-mail: gfduan@zju.edu.cn)

Abstract

In this study, a novel refined plate theory (RPT) is developed for the static analysis of FG plates, which is a simplification of the higher-order shear deformation theories (HSDTs). It improves the computational efficiency while preserving the accuracy advantage of HSDTs. The C1-continuity problem is overcome by isogeometric analysis (IGA), which shows more advantages than the C0 elements based finite element analysis. By T-splines, the computational costis effectively reduced, since compared to NURBS based IGA, T-splines can achieve local refinement and improve the utilization of control points. The rule of mixture with power-law and Mori–Tanaka scheme are adopted to calculate the material properties of the plate. Several numerical experiments are given to prove the efficiency of the proposed method.

Keywords FG Plates; Static bending; Refined plate theory; T-splines; Isogeometric analysis;

1. Introduction

Functional gradient plate (FG plate) is a new composite structure, which is usually composed of ceramic and metal materials. Due to the smooth and continuous change of material components in a certain direction, FG plate can eliminate the interlaminar stress of composite materials. Thus the FG plates overcome the delamination or debonding problems since there are no material interfaces. In addition, FG plate has the characteristics of high temperature resistance, high insulation, good strength and wear resistance. Due to these superior properties, they are widely used in ships, vehicles, aircrafts, etc [1].

In practical applications, the static bending behaviors of the plate are very important for structural design. Besides, shear deformation has significant effects on the response of FG plates. However, most of current methods are based on classical plate theory (CPT) and first-order shear deformation theory (FSDT) [2], [3]. Such methods can not reflect the change of the shear strain in the plate thickness. To solve this problem, several higher-order shear deformation theories (HSDTs) are developed. Such as third order deformation theory (TSDT) [4]-[6], fifth-order shear deformation theory (FiSDT) [7], hyperbolic shear deformation theory (HySDT) [8]-[10], exponential shear deformation theory (ESDT) [11]-[13], trigonometric shear deformation theory (TrSDT) [14]-[16] and so on.

In addition, Senthilnathan et al. [17] simplifies TSDT and develop refined plate theory (RPT), which requires one less unknown variable than TSDT but preserve the accuracy advantage. Later, RPT models for the analysis of isotropic and orthotropic plates are developed [18]-[20]. However, in traditional C0-continuity finite element analysis (FEA), C1-continuity requirement of RPT is a big problem. In order to solve the continuity problem, some C0 approximations [21]-[23] and Hermite interpolation [4] methods are developed, but these methods require more variables. In particular, each node used in [24] has 10 degrees of freedom (DOF), which increases the computational complexity.

Recently, Hughes et al. [25] developed isogeometric analysis (IGA) by using spline basis functions as analysis tools. Because spline basis functions can achieve high-order continuity, it is easy for IGA to solve the C1-continuity problem. More importantly, only four DOFs are required for each control point in proposed method. Besides, the splines can be directly used to construct the geometric models, so as to solve the data communication problem. IGA has solved many engineering problems, such as solid mechanics [26], [27], fluid mechanics [28] and contact mechanics [29]. The static [30]-[32], free vibration [33]-[35] and buckling [36], [37] analysis of FG plates are also involved.

However, traditional IGA is based on NURBS, which is inefficient in the representation of detail local features [38]. T-splines overcome the shortcomings because they allow local refinement and coarsening, which highly improves the utilization of control points. This is important because fewer control points mean faster modeling time and higher analytical efficiency. Nevertheless, T-splines are not always used directly in analysis for different geometric configurations, because they are not necessarily linearly independent and partition of unity of the polynomial basis functions is not satisfied. Li et al. [39] introduced analysis-suitable T-splines (ASTS), wherein the linear independence of its basis functions is always satisfied. Moreover, Scott MA et al. [40] develop a local refinement algorithm for ASTS, Da Veiga LB et al. [41] define ASTS of arbitrary degree and prove fundamental properties.

In this paper, T-splines based IGA together with RPT is developed to investigate the static behavior of FG plates. An efficient RPT model based on the hyperbolic function is also developed, and proposed model has more expressions than traditional RPT because it can be expressed by Taylor expansion. Compared with HSDTs, RPT reduces one unknown variable at each control point to improve computational efficiency. IGA can easily solve higher order continuity problem in traditional FEA. Furthermore, the superior features of T-splines can tower over traditional NURBS based IGA, since it can achieve local refinement and improve the utilization of control points, which effectively reduce the computational cost. Since the rule of mixture in the previous work [42], [43] cannot reflect the interactions among constituents, the Mori–Tanaka scheme is also adopted to calculate the effective material properties.

2. A novel refined plate theory for FG plates

2.1 Functionally graded plates

The geometry model of FG plate is shown in Figure 1, in which the material properties graded through the plate thickness. The rule of mixture with power-law [44] is used to construct the material model of the plate

$$V_c(z) = \left(\frac{1}{2} + \frac{z}{h}\right)^n, \quad V_m = 1 - V_c, \quad z \in \left[-h/2, h/2\right] \tag{1}$$

where V is the volume fraction, h is the thickness of the plate, n is the material index. In all of the following equations, the metal and ceramic components are represented by subscripts m and c. Based on the rule of mixture

$$
\begin{aligned}
E_e &= E_m V_m + E_c V_c \\
v_e &= v_m V_m + v_c V_c
\end{aligned}
\tag{2}
$$

where E_e and v_e are the effective Young's modulus and the Poisson's ratio. Notes that on the boundary $z=0$ and $z=h$, the material is fully ceramic and metal, respectively.

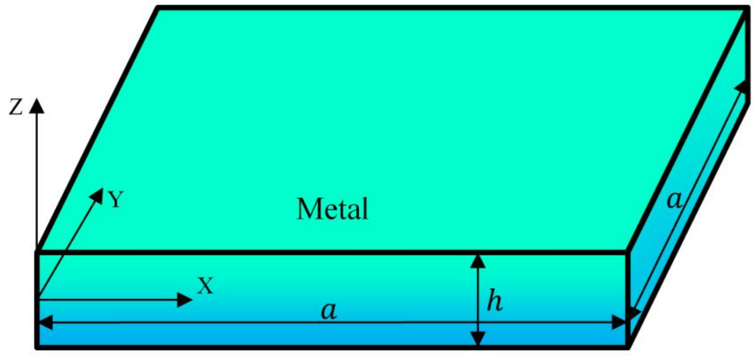

Figure 1. Geometry model of FG plate

However, the rule of mixture cannot reflect the interactions among constituents. Therefore, Mori-Tanaka scheme [45] is adopted to overcome this problem

$$
\frac{K_e - K_m}{K_c - K_m} = \frac{V_c}{1 + V_m \frac{K_c - K_m}{K_m + 4G_m/3}}, \quad \frac{G_e - G_m}{G_c - G_m} = \frac{V_c}{1 + V_m \frac{G_c - G_m}{G_m + f_1}} \tag{3}
$$

where G_e is modulus of shear and K_e is modulus of bulk, the parameter is defined as

$$
f_1 = \frac{G_m (9K_m + 8G_m)}{6(K_m + 2G_m)} \tag{4}
$$

then

$$
E_e = \frac{9K_e G_e}{3K_e + G_e}, \quad v_e = \frac{3K_e - 2G_e}{2(3K_e + G_e)} \tag{5}
$$

Figure 2 shows the change of the effective modulus of Al/Al_2O_3 with the power index n. The results computed by the rule of mixture are smaller than the Mori-Tanaka scheme.

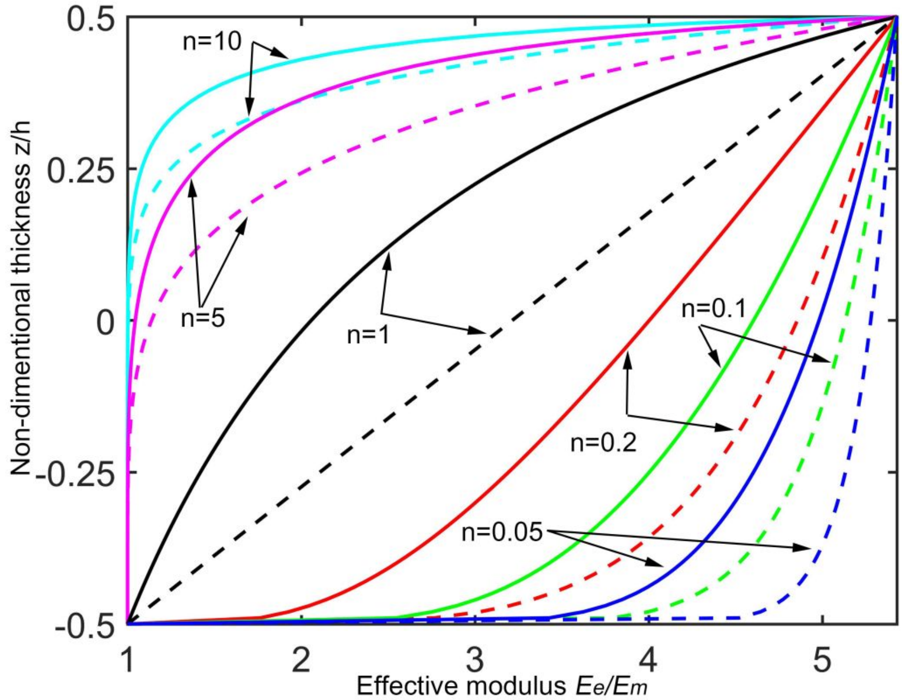

Figure 2. The effective modulus of Al/Al_2O_3 plate computed by the Mori-Tanaka technique (solid lines) and rule of mixture (dash lines).

2.2 FG plates formulation based on RPT

Based on the TSDT, the displacement field for the bending plates is described as

$$\begin{cases} u_\Omega = u_0 + z\beta_x + g(z)\left(w_{0,x} + \beta_x\right) \\ v_\Omega = v_0 + z\beta_y + g(z)\left(w_{0,y} + \beta_y\right) \\ w_\Omega = w_0 \end{cases} \quad z \in \left[\frac{-h}{2}, \frac{h}{2}\right] \tag{6}$$

where $g(z) = -4z^3/3h^2$ is the shape function, u_0, v_0 and w_0 are the mid-plane displacements of the plate, β_x and β_y are the transverse normal rotations of the plate. The subscripts $,x$ and $,y$ is defined as derivatives of *x* and *y*.

Then, decomposing the mid-plane displacement w_0 into the bending part w_b and the shear part w_s, the transverse normal rotations can be defined as the derivative of w_b

$$w_0 = w_b + w_s, \quad \boldsymbol{\beta} = -\nabla w_b \tag{7}$$

Substituting Eq. (7) into Eq.(6), the displacement fields can be transformed into the RPT form.

$$\begin{cases} u_\Omega = u_0 - z w_{b,x} + g(z) w_{s,x} \\ v_\Omega = v_0 - z w_{b,y} + g(z) w_{s,y} \\ w_\Omega = w_b + w_s \end{cases} \tag{8}$$

thus the unknown variables are reduced from five to four. Several shape functions $g(z)$ in exist literatures [4], [7], [12], [16] are list in Table 1, their distributions and detectives are shown in Figure 3. In this paper, a new shape function is proposed by the combination of hyperbolic function and linear function.

Table 1. Different shape functions

Model	$g(z)$
Reddy (TSDT) [4]	$-4z^3/3h^2$
Nguyen-Xuan (FiSDT) [7]	$-z/8-2z^3/h^2+2z^5/h^4$
Karama (ESDT) [12]	$ze^{-2(z/h)^2}-z$
Thai (ITSDT) [16]	$h\arctan(2z/h)-2z$
Present	$-ze^{-1}\cosh(2z/h)$

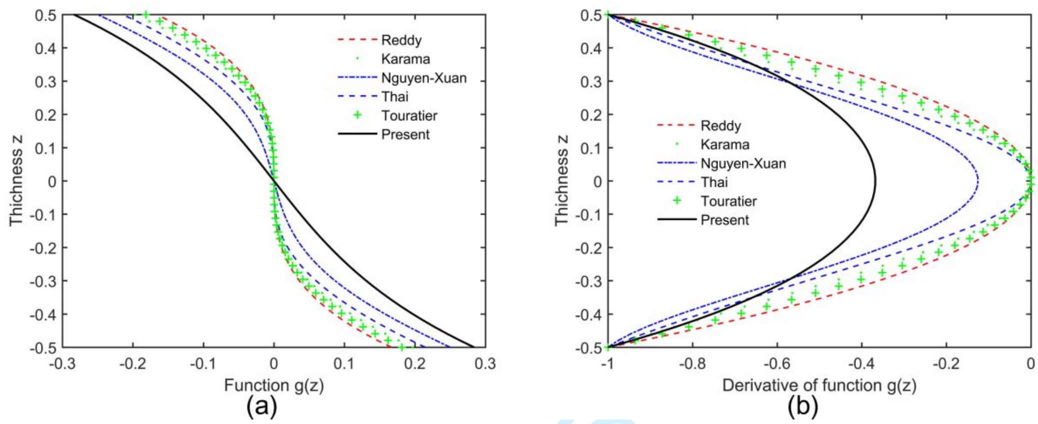

Figure 3. Shape functions and their derivatives through the plate thickness.

The strain $\boldsymbol{\varepsilon}$ associated with the displacements field in Eq. (8) can be obtained

$$\begin{aligned}\boldsymbol{\varepsilon} &= \boldsymbol{\varepsilon}_0 + z\boldsymbol{\kappa}_b + g(z)\boldsymbol{\kappa}_s \\ \boldsymbol{\gamma} &= \left(g'(z)+1\right)\boldsymbol{\varepsilon}_s\end{aligned} \tag{9}$$

where

$$\boldsymbol{\varepsilon} = \begin{bmatrix}\varepsilon_{xx}\\ \varepsilon_{yy}\\ \varepsilon_{xy}\end{bmatrix}, \boldsymbol{\varepsilon}_0 = \begin{bmatrix}u_{0,x}\\ v_{0,y}\\ u_{0,y}+v_{0,x}\end{bmatrix}, \boldsymbol{\kappa}_b = -\begin{bmatrix}w_{b,xx}\\ w_{b,yy}\\ 2w_{b,xy}\end{bmatrix}, \boldsymbol{\kappa}_s = \begin{bmatrix}w_{s,xx}\\ w_{s,yy}\\ 2w_{s,xy}\end{bmatrix} \tag{10}$$

$$\boldsymbol{\gamma} = \begin{bmatrix}\gamma_{xz}\\ \gamma_{yz}\end{bmatrix}, \boldsymbol{\varepsilon}_s = \begin{bmatrix}w_{s,x}\\ w_{s,y}\end{bmatrix} \tag{11}$$

Base on the Hooke's law, the linear constitutive relation of FG plates are given by

$$\begin{bmatrix} \sigma_{xx} \\ \sigma_{yy} \\ \tau_{xy} \\ \tau_{xz} \\ \tau_{yz} \end{bmatrix} = \begin{bmatrix} Q_{11} & Q_{12} & 0 & 0 & 0 \\ & Q_{22} & 0 & 0 & 0 \\ & & Q_{33} & 0 & 0 \\ & & & Q_{55} & 0 \\ sym & & & & Q_{44} \end{bmatrix} \begin{bmatrix} \varepsilon_{xx} \\ \varepsilon_{yy} \\ \gamma_{xy} \\ \gamma_{xz} \\ \gamma_{yz} \end{bmatrix} \tag{12}$$

where

$$\begin{aligned} Q_{11} &= Q_{22} = \frac{E_e}{1-v_e^2}, Q_{12} = \frac{v_e E_e}{1-v_e^2} \\ Q_{33} &= Q_{44} = Q_{55} = \frac{E_e}{2(1+v_e)} \end{aligned} \tag{13}$$

The weak form for static bending problem of the FG plate is

$$\int_\Omega \delta \boldsymbol{\varepsilon}_\mathbf{b}^\mathrm{T} \mathbf{D}_\mathbf{b} \boldsymbol{\varepsilon}_\mathbf{b} d\Omega + \int_\Omega \delta \boldsymbol{\varepsilon}_\mathbf{s}^\mathrm{T} \mathbf{D}_\mathbf{s} \boldsymbol{\varepsilon}_\mathbf{s} d\Omega = \int_\Omega \delta(w_b + w_s) q_0 d\Omega \tag{14}$$

where

$$\boldsymbol{\varepsilon}_\mathbf{b} = \begin{bmatrix} \boldsymbol{\varepsilon}_\mathbf{0} \\ \boldsymbol{\kappa}_\mathbf{b} \\ \boldsymbol{\kappa}_\mathbf{s} \end{bmatrix}, \boldsymbol{\varepsilon}_\mathbf{s} = \begin{bmatrix} w_{s,x} \\ w_{s,y} \end{bmatrix} \tag{15}$$

where $\boldsymbol{\varepsilon}_\mathbf{b}$ and $\boldsymbol{\varepsilon}_\mathbf{s}$ are the bending stain and the shear strain, respectively. $\mathbf{D}_\mathbf{b}$ and $\mathbf{D}_\mathbf{s}$ is the material matrix, which can be defined as

$$\mathbf{D}_\mathbf{b} = \begin{bmatrix} \mathbf{A} & \mathbf{B} & \mathbf{E} \\ \mathbf{B} & \mathbf{D} & \mathbf{F} \\ \mathbf{E} & \mathbf{F} & \mathbf{H} \end{bmatrix}, \mathbf{D}_\mathbf{s} = \int_{-h/2}^{h/2} \left(g'(z)+1\right)^2 \mathbf{G} dz \tag{16}$$

with

$$(\mathbf{A}, \mathbf{B}, \mathbf{D}, \mathbf{E}, \mathbf{F}, \mathbf{H}) = \int_{-h/2}^{h/2} \left(1, z, z^2, g(z), zg(z), g(z)^2\right) \mathbf{Q} dz \tag{17}$$

where

$$\mathbf{G} = \frac{E_e}{2(1+v_e)} \begin{bmatrix} 1 & 0 \\ 0 & 1 \end{bmatrix}, \quad \mathbf{Q} = \frac{E_e}{1-v_e^2} \begin{bmatrix} 1 & v_e & 0 \\ v_e & 1 & 0 \\ 0 & 0 & (1-v_e)/2 \end{bmatrix} \tag{18}$$

3. T-splines based isogeometric analysis

3.1 ASTS and Bézier extraction

T-spline is the latest modeling technology proposed in 2003 [46], It not only inherits the advantages of traditional NURBS, but also solves the problem of surface subdivision. Although it is very similar to NURBS, it greatly reduces the number of control points on the surface of the model. This feature is of great significance to improve the speed of modeling and analysis. More technical details on T-Splines can be found in Ref [47], [48]. With NURBS, global knot vectors are used to define all basis functions. For T-splines, basis function is calculated by its local knot vector, thus T-splines allow local refinement. T-splines are constructed from a T-mesh with T-junctions. When there are no T-junctions in the T-mesh, T-splines is degenerate to a NURBS. ASTS are a subset of T-splines with a restricted T-mesh topology [49]. By extending the two lines of the T-junctions (the red lines in Figure 4(a)), the T-mesh of ASTS can be formed. Figure 4(b) shows the extension result of the T-splines in (s,t) parameter space.

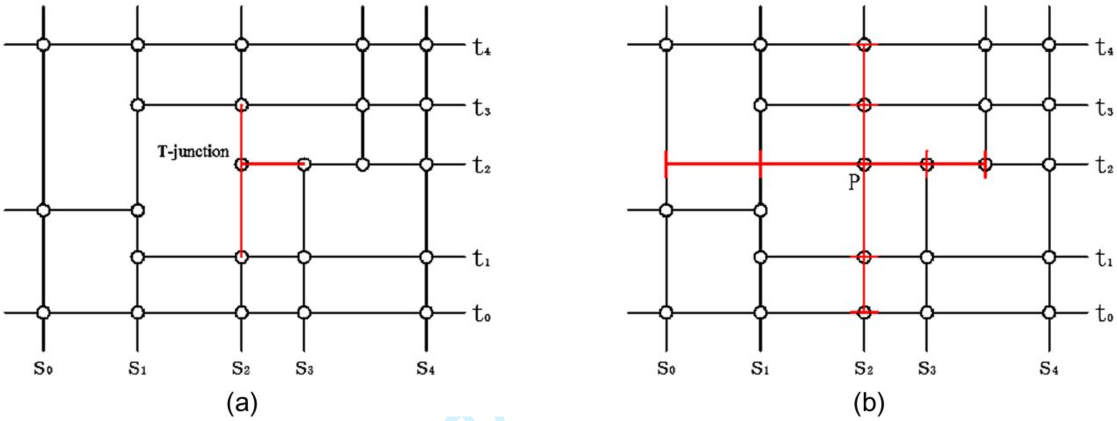

Figure 4. T-mesh: (a) T-junctions, (b) knot lines of the basis function $\mathrm{T}^{\mathrm{P}}(s,t)$

As is shown in Figure 4(b), ASTS basis function of point P in the T-mesh can be defined as [50]

$$\mathbf{T}_i(s,t) = \mathrm{T}_i(s) \otimes \mathrm{T}_i(t) \tag{19}$$

where $\mathrm{T}_i(s)$ and $\mathrm{T}_i(t)$ are the basis functions of following knot vectors

$$\mathbf{s}_i = [s_{i0} \quad s_{i1} \quad s_{i2} \quad s_{i3} \quad s_{i4}] \text{ and } \mathbf{t}_i = [t_{i0} \quad t_{i1} \quad t_{i2} \quad t_{i3} \quad t_{i4}] \tag{20}$$

, respectively. Knot vector $\mathbf{s}_i$ and $\mathbf{t}_i$ can be extracted from the T-mesh. By introducing knot weight factors ω_i, the rational ASTS basis function is defined as

$$R_i(s,t) = \frac{\mathrm{T}_i(s,t)\omega_i}{\sum_{j=0}^{n} \mathrm{T}_j(s,t)\omega_j} \tag{21}$$

thus a ASTS surface is define as

$$S = \sum_{i=1}^{m\times n} R_i(s,t)\mathbf{P}_i \tag{22}$$

where $\mathbf{P}_i = [x, y]_i$ is the control point of the surface in physical space.

The Bézier extraction is applied to incorporate ASTS into the existing IGA framework, this ensures that the ASTS are compatible with NURBS. It is defined as

$$\mathbf{T}^e(s,t)=\mathbf{C}^e\mathbf{G}(s,t) \tag{23}$$

where $\mathbf{T}^e$ is ASTS basis function, $\mathbf{C}^e$ is Bézier extraction operator of element *e*. $\mathbf{G}(s,t)$ is the Bernstein polynomial defined on parent element [-1,1]

$$\begin{aligned} G_{i,p}(t) &= \frac{1}{2^p}\binom{p}{i-1}(1-t)^{p-(i-1)}(1+t)^{i-1} \\ \mathbf{G}(s,t) &= G(s)\otimes G(t) \end{aligned} \tag{24}$$

where

$$\binom{p}{i-1}=\frac{p!}{(i-1)!(p+1-i)!} \tag{25}$$

Note that, $\mathbf{G}(s,t)$ is same for all the ASTS elements. Substituting Eq. (23) into Eq. (21) and writing it in matrix form

$$\mathbf{R}^e(s,t)=\frac{\mathbf{W}^e\mathbf{T}(s,t)}{\mathrm{W}(s,t)},\ \mathrm{W}(s,t)=(\mathbf{w}^e)^T\mathbf{C}^e\mathbf{G} \tag{26}$$

where $\mathbf{w}^e$ is the weight for ASTS, its diagonal matrix is $\mathbf{W}$.

3.2 RPT formulation based on IGA

In IGA, both geometric model and its analytical model are constructed by ASTS. Since ASTS can construct higher-order elements, C1-continuity requirement of RPT is solved. The deflection fields of the FG plate are

$$\mathbf{u}^e=\sum_{i=1}^{m\times n}R_i^e(s,t)\mathbf{q}_i^e \tag{27}$$

where $R_A(\xi,\eta)$ is the basis function defined in Eq. (26), $\mathbf{q}_A=\begin{bmatrix}u_{0A} & v_{0A} & w_{bA} & w_{sA}\end{bmatrix}^T$ is the displacement vector. Substituting Eq. (27) into Eqs. (10) and (11), the strains of the plate are

$$\begin{bmatrix}\boldsymbol{\varepsilon}_0^T & \boldsymbol{\kappa}_b^T & \boldsymbol{\kappa}_s^T & \boldsymbol{\varepsilon}_s^T\end{bmatrix}^T=\sum_{i=1}^{m\times n}\begin{bmatrix}(\mathbf{B}^m)^T & (\mathbf{B}^{b1})^T & (\mathbf{B}^{b2})^T & (\mathbf{B}^s)^T\end{bmatrix}_i^T\mathbf{q}_i \tag{28}$$

where

$$\begin{aligned} \mathbf{B}^m &= \begin{bmatrix} R_{,x} & 0 & 0 & 0 \\ 0 & R_{,y} & 0 & 0 \\ R_{,y} & R_{,x} & 0 & 0 \end{bmatrix}, \mathbf{B}^{b1} = -\begin{bmatrix} 0 & 0 & R_{,xx} & 0 \\ 0 & 0 & R_{,yy} & 0 \\ 0 & 0 & 2R_{,xy} & 0 \end{bmatrix}, \\ \mathbf{B}^{b2} &= \begin{bmatrix} 0 & 0 & 0 & R_{,xx} \\ 0 & 0 & 0 & R_{,yy} \\ 0 & 0 & 0 & 2R_{,xy} \end{bmatrix}, \mathbf{B}^s = \begin{bmatrix} 0 & 0 & 0 & R_{,x} \\ 0 & 0 & 0 & R_{,y} \end{bmatrix} \end{aligned} \tag{29}$$

The derivatives of $\mathbf{R}$ to the parameter space, (s,t) is

$$\begin{aligned}\mathbf{R}_{,s} &= \mathbf{W}^e\mathbf{C}^e\left(\frac{\mathbf{G}_{,s}}{\mathrm{W}} - \frac{\mathrm{W}_{,s}\mathbf{G}}{\mathrm{W}^2}\right)\\ \mathbf{R}_{,st} &= \mathbf{W}^e\mathbf{C}^e\left(\frac{\mathbf{G}_{,st}}{\mathrm{W}} - \frac{\mathrm{W}_{,t}\mathbf{G}_{,s} - \mathrm{W}_{,s}\mathbf{G}_{,t} - \mathrm{W}_{,st}\mathbf{G}}{\mathrm{W}^2} + \frac{2\,\mathrm{W}_{,s}\mathrm{W}_{,t}\mathbf{G}}{\mathrm{W}^3}\right)\end{aligned} \tag{30}$$

To compute the derivatives of $\mathbf{R}$ to the physical space, (x,y), chain rule of differentiation is applied as

$$\begin{bmatrix}\mathbf{R}_{,x}\\ \mathbf{R}_{,y}\end{bmatrix} = \mathbf{J}_1^{-1}\begin{bmatrix}\mathbf{R}_{,s}\\ \mathbf{R}_{,t}\end{bmatrix},\quad \begin{bmatrix}\mathbf{R}_{,xx}\\ \mathbf{R}_{,yy}\\ \mathbf{R}_{,xy}\end{bmatrix} = \mathbf{J}_3^{-1}\left(\begin{bmatrix}\mathbf{R}_{,ss}\\ \mathbf{R}_{,tt}\\ \mathbf{R}_{,st}\end{bmatrix} - \mathbf{J}_2\begin{bmatrix}\mathbf{R}_{,x}\\ \mathbf{R}_{,y}\end{bmatrix}\right) \tag{31}$$

where Jacobian matrix, $(\mathbf{J}_1, \mathbf{J}_2, \mathbf{J}_3)$ are computed as

$$\mathbf{J}_1 = \begin{bmatrix}x_{,s} & y_{,s}\\ x_{,t} & y_{,t}\end{bmatrix},\quad \mathbf{J}_2 = \begin{bmatrix}x_{,ss} & y_{,ss}\\ x_{,tt} & y_{,tt}\\ x_{,st} & y_{,st}\end{bmatrix},\quad \mathbf{J}_3 = \begin{bmatrix}(x_{,s})^2 & (y_{,s})^2 & 2x_{,s}y_{,s}\\ (x_{,t})^2 & (y_{,t})^2 & 2x_{,t}y_{,t}\\ x_{,s}x_{,t} & y_{,s}y_{,t} & x_{,s}y_{,t} + x_{,t}y_{,s}\end{bmatrix} \tag{32}$$

Substituting Eq. (28) into Eq. (14), the equilibrium equations for static bending problem of FG plates can be obtained

$$\mathbf{Kq} = \mathbf{F} \tag{33}$$

where $\mathbf{K}$ is global stiffness matrix, $\mathbf{F}$ is load vector, calculated by

$$\mathbf{F} = \int_\Omega q_0 \begin{bmatrix}0 & 0 & R & R\end{bmatrix}^T d\Omega \tag{34}$$

$$\mathbf{K} = \int_\Omega \left(\begin{bmatrix}\mathbf{B}^m\\ \mathbf{B}^{b1}\\ \mathbf{B}^{b2}\end{bmatrix}^T \mathbf{D}_b \begin{bmatrix}\mathbf{B}^m\\ \mathbf{B}^{b1}\\ \mathbf{B}^{b2}\end{bmatrix} + \left(\mathbf{B}^s\right)^T \mathbf{D}_s\mathbf{B}^s\right) d\Omega \tag{35}$$

where

$$\mathbf{B}^g = \begin{bmatrix}0 & 0 & R_{,x} & R_{,x}\\ 0 & 0 & R_{,y} & R_{,y}\end{bmatrix} \tag{36}$$

3.3 Essential boundary conditions

Based on IGA, the four edges simply supported boundary condition (BC) is enforced in the same way as the traditional FEA

Simply supported (SSSS):

$$
\begin{aligned}
u_0 = w_b = w_s = 0 \ \text{ at } x = 0, a, \\
v_0 = w_b = w_s = 0 \ \text{ at } y = 0, b.
\end{aligned} \tag{37}
$$

the BCs of u_0, v_0, w_b and w_s can be processed directly, which is an advantage over most meshless methods that usually do not provide Kronecker Delta properties [51]. For the four edges clamped, the BCs can be enforced as

Clamped (CCCC):

$$
u_0 = v_0 = w_b = w_s = w_{b,n} = w_{s,n} = 0 \tag{38}
$$

Because the normal slopes $w_{b,n}$ and $w_{s,n}$ are not approximate in IGA, they cannot be imposed directly. An alternative way [52] to solve the boundary problem is to fix the boundary points and their adjacent points. Compared with other methods [53], [54], this way is much simpler

4. Results and discussions

4.1 Convergence study

Figure 5 shows an Al/Al_2O_3 square plate with a uniform load q_0 on its top surface. Table 2 lists the material properties used in proposed work. Defined the non-dimensional central deflection

$$
\overline{w} = \frac{E_m}{q_0 h} w\left(\frac{a}{2}, \frac{a}{2}, 0\right) \tag{39}
$$

The displacement convergence diagram of the Al/Al_2O_3 plate is shown in Figure 6. The material index n=1 and thickness-to-width ratio h/a=0.1. It can be seen that T-splines and cubic NURBS can result in better convergence, but as is shown in Table 3, the control points required in T-splines model are quite less than that in the cubic NURBS, this is important because fewer control points means faster modeling time and higher analytical efficiency. To balance accuracy and efficiency, T-splines with 412 elements is adopted for the later study.

Table 2. Material Properties

Property	Material			
	Al	Al_2O_3	ZrO_2-1	ZrO_2-2
E(Gpa)	70	380	200	151
v	0.3	0.3	0.3	0.3

Table 3. Elements type

Elements type	Num of Elements	Control Points	E/P Rate
T-splines	412	409	1.007
quadratic NURBS	400	484	0.826
cubic NURBS	400	529	0.759

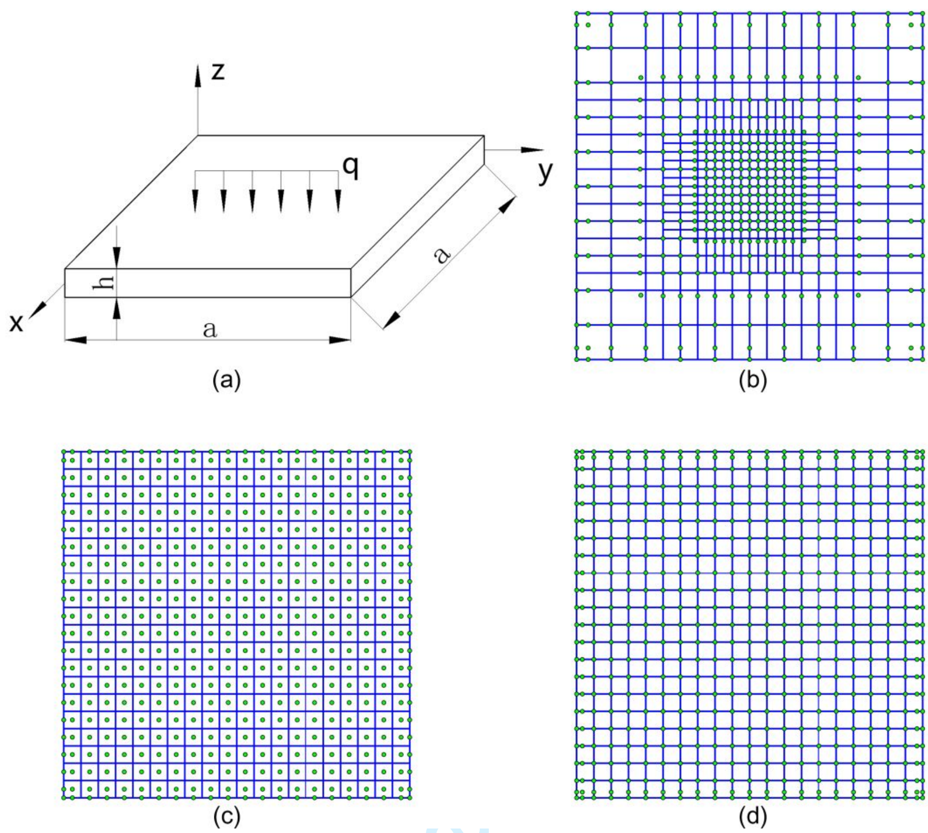

Figure 5. (a) geometry model (b) T-splines elements (c) quadratic NURBS elements (d) cubic NURBS elements.

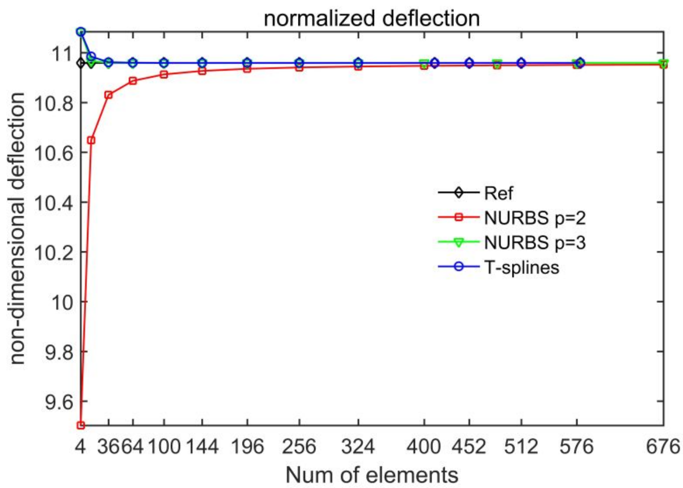

Figure 6. Convergence study of the simply supported (SSSS) Al/Al_2O_3 plate.

4.2 Static analysis

4.2.1 Square plate static analysis

In this example, an Al/ZrO_2-1 square plate under a uniform load q_0 on its top surface is discussed. The deflections of the FG plate under three different boundary conditions are shown in Figure 7, in which $n=1$ and h/a=0.1. Mori-Tanaka scheme is used to calculate the effective properties of the plate.

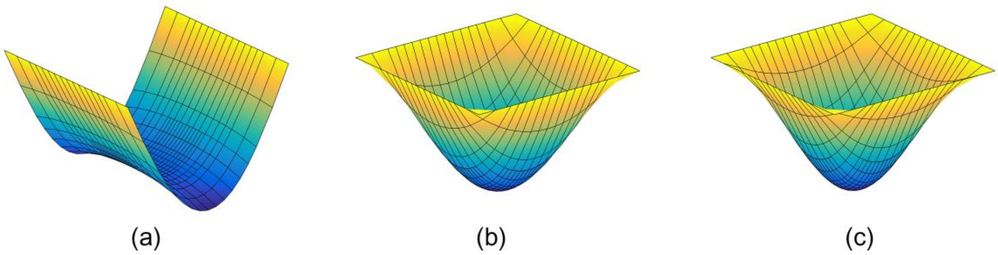

Figure 7. Deflection shapes of Al/ZrO_2-1 plate. (a) SFSF, (b) SSSS, (c) CCCC.

The deflections of Al/ZrO_2-1 plate with thickness-to-width ratio h/a=0.1 based on proposed method and several other techniques are list in Table 4. The material index has a positive effect on the plate central deflections, because a larger material index means more metal composition, which leads to a decrease in the plate stiffness.

Table 4. Non-dimensional deflections of Al/ZrO_2-1 plate, in which h/a=0.1.

BCs	n	Model				
		TSDT[4]	FiSDT[7]	ESDT[12]	ITSDT[16]	present
SFSF	ceramic	5.874E+2	5.871E+2	5.873E+2	5.872E+2	5.874E+2
	0.1	6.669E+2	6.667E+2	6.669E+2	6.667E+2	6.669E+2
	0.2	7.260E+2	7.257E+2	7.259E+2	7.257E+2	7.260E+2
	1	9.468E+2	9.465E+2	9.467E+2	9.465E+2	9.468E+2
	5	1.199E+3	1.199E+3	1.199E+3	1.199E+3	1.199E+3
	10	1.328E+3	1.327E+3	1.328E+3	1.327E+3	1.328E+3
	metal	1.678E+3	1.678E+3	1.678E+3	1.678E+3	1.678E+3
SSSS	ceramic	1.633E+2	1.632E+2	1.633E+2	1.632E+2	1.633E+2
	0.1	1.855E+2	1.853E+2	1.854E+2	1.853E+2	1.855E+2
	0.2	2.022E+2	2.020E+2	2.021E+2	2.021E+2	2.022E+2
	1	2.669E+2	2.667E+2	2.668E+2	2.667E+2	2.668E+2
	5	3.379E+2	3.377E+2	3.379E+2	3.377E+2	3.379E+2
	10	3.723E+2	3.718E+2	3.721E+2	3.719E+2	3.723E+2
	metal	4.666E+2	4.662E+2	4.664E+2	4.662E+2	4.666E+2
CCCC	ceramic	5.589E+1	5.574E+1	5.583E+1	5.576E+1	5.589E+1
	0.1	6.351E+1	6.335E+1	6.345E+1	6.337E+1	6.351E+1
	0.2	6.962E+1	6.944E+1	6.955E+1	6.946E+1	6.962E+1
	1	9.539E+1	9.516E+1	9.531E+1	9.520E+1	9.538E+1
	5	1.207E+2	1.204E+2	1.206E+2	1.204E+2	1.206E+2
	10	1.308E+2	1.303E+2	1.306E+2	1.304E+2	1.308E+2
	metal	1.597E+2	1.593E+2	1.595E+2	1.593E+2	1.597E+2

Table 5 list the deflections of Al/ZrO_2-1 plate, in which material index $n=1$. The deflections of the plate increase rapidly with the decrease of thickness-to-width ratios. This is because the plate stiffness decreases with the decrease of thickness-to-width ratios. Figure 8 shows the stress variation in the thickness direction of the plate with clamped edges. Axial stress on the bottom (metal) surface is smaller than that on the top (ceramic) surface of plate. Material indexes will affect the stress distribution patterns of the plate

Table 5. Non-dimensional deflections of Al/ZrO_2-1 plate, in which $n = 1$.

BCs	*h/a*	Model				
		TSDT[4]	FiSDT[7]	ESDT[12]	ITSDT[16]	present
SFSF	0.2	6.349E+1	6.341E+1	6.347E+1	6.342E+1	6.349E+1
	0.1	9.468E+2	9.465E+2	9.467E+2	9.465E+2	9.468E+2
	0.05	1.487E+4	1.487E+4	1.487E+4	1.487E+4	1.487E+4
	0.02	5.779E+5	5.779E+5	5.779E+5	5.779E+5	5.779E+5
SSSS	0.2	1.922E+1	1.917E+1	1.920E+1	1.917E+1	1.922E+1
	0.1	2.669E+2	2.667E+2	2.668E+2	2.667E+2	2.668E+2
	0.05	4.107E+3	4.106E+3	4.106E+3	4.106E+3	4.107E+3
	0.02	1.586E+5	1.586E+5	1.586E+5	1.586E+5	1.586E+5
CCCC	0.2	8.313	8.231	8.278	8.241	8.314
	0.1	9.539E+1	9.516E+1	9.531E+1	9.520E+1	9.538E+1
	0.05	1.374E+3	1.373E+3	1.373E+3	1.373E+3	1.374E+3
	0.02	5.198E+4	5.198E+4	5.198E+4	5.198E+4	5.198E+4

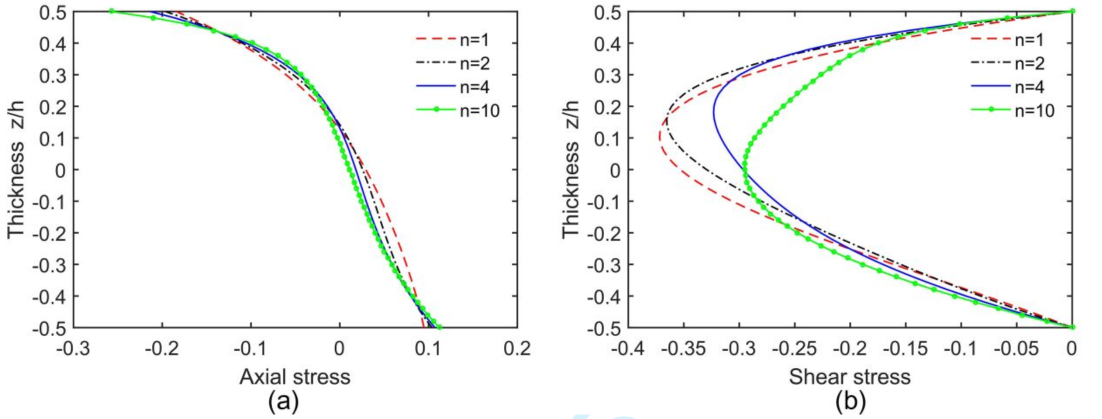

Figure 8. The **s**tresses through plate thickness with *h/a*=0.2 and CCCC boundary condition.

4.2.2 Prismatic plate static analysis

In this example, the static analysis of an Al/ZrO_2-2 prismatic plate is conducted, the plate geometry is built by T-splines with 412 elements, as shown in Figure 9. The deflection shapes of plate is shown in Figure 10, in which the thickness-to-width *h/a*=0.1 and material index n=1. The same as squire plate, the effective properties is calculated by Mori-Tanaka scheme.

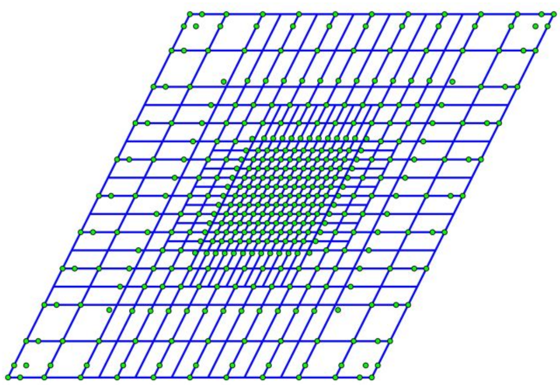

Figure 9. Mesh of prismatic plate.

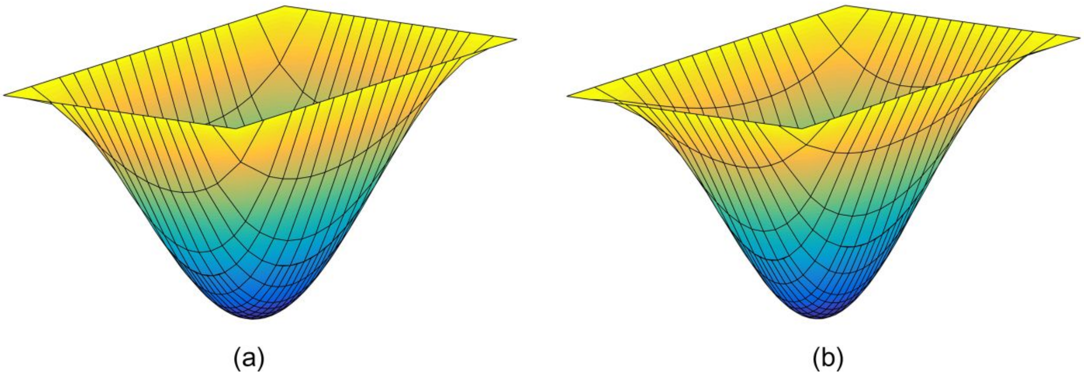

Figure 10. Deflection shapes of Al/ZrO_2-2 prismatic plate. (a) SSSS, (b) CCCC.

The non-dimensional deflections of Al/ZrO_2-2 prismatic plate are list in Table 6. The effectiveness of proposed method is still guaranteed in the prismatic plate model. Figure 11 shows the influence of material indexes on the non-dimensional deflection of prismatic plate. Table 7 shows the non-dimensional deflections of Al/ZrO_2-2 prismatic plate, in which material index n=1. The Stress distributions through the plate thickness under CCCC boundary condition are shown in Figure 12. The prismatic plate has a similar stress variation tendency as the square plate.

Table 6. Non-dimensional deflections of Al/ZrO_2-2 prismatic plate, in which h/a=0.2.

BCs	n	Model				
		TSDT[4]	FiSDT[7]	ESDT[12]	ITSDT[16]	present
SSSS	ceramic	13.480	13.434	13.463	13.440	13.480
	0.1	14.695	14.646	14.677	14.653	14.695
	0.2	15.646	15.594	15.626	15.601	15.646
	1	19.439	19.376	19.417	19.385	19.438
	5	23.542	23.469	23.521	23.481	23.539
	10	25.174	25.068	25.134	25.082	25.175
	metal	29.079	28.979	29.042	28.993	29.078
CCCC	ceramic	5.606	5.539	5.576	5.546	5.608
	0.1	6.086	6.015	6.054	6.022	6.088
	0.2	6.481	6.405	6.447	6.413	6.483
	1	8.239	8.143	8.197	8.155	8.241
	5	10.208	10.087	10.158	10.103	10.210
	10	10.803	10.649	10.733	10.667	10.808
	metal	12.093	11.948	12.028	11.964	12.098

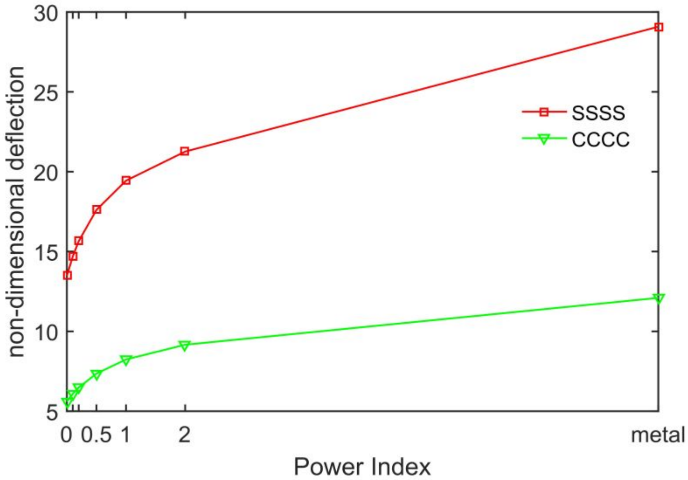

Figure 11. Influence of material indexes on the non-dimensional deflection of Al/ZrO_2-2 prismatic plate

Table 7. Non-dimensional deflections of Al/ZrO_2-2 prismatic plate, in which n=1.

BCs	*h/a*	Model				
		TSDT[4]	FiSDT[7]	ESDT[12]	ITSDT[16]	present
SSSS	0.2	1.944E+1	1.938E+1	1.942E+1	1.939E+1	1.944E+1
	0.1	2.678E+2	2.676E+2	2.678E+2	2.676E+2	2.678E+2
	0.05	4.112E+3	4.112E+3	4.112E+3	4.112E+3	4.112E+3
	0.02	1.587E+5	1.587E+5	1.587E+5	1.587E+5	1.587E+5
CCCC	0.2	8.239	8.143	8.197	8.155	8.241
	0.1	9.196E+1	9.170E+1	9.187E+1	9.174E+1	9.196E+1
	0.05	1.310E+3	1.309E+3	1.309E+3	1.309E+3	1.309E+3
	0.02	4.937E+4	4.937E+4	4.937E+4	4.937E+4	4.937E+4

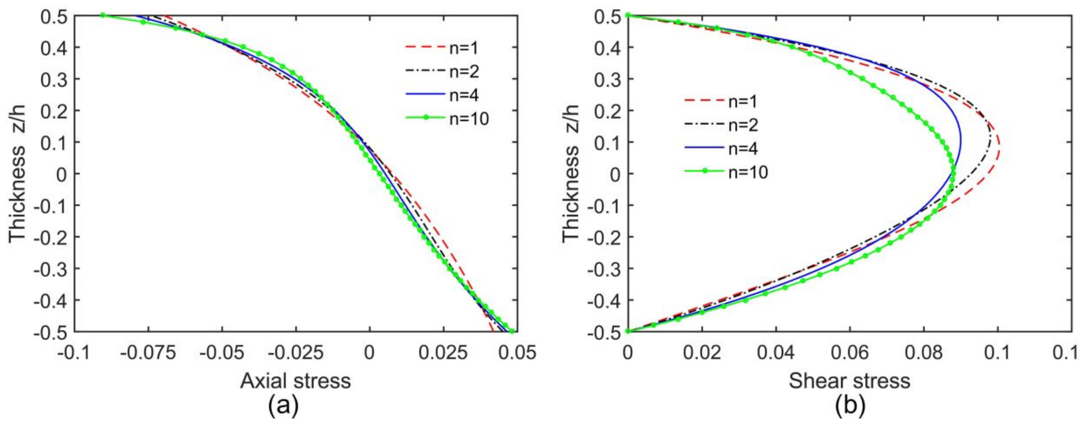

Figure 12. Stresses distribution through the plate thickness with *h/a*=0.2 and CCCC boundary condition.

5. Conclusion

In this paper, the RPT and T-splines based IGA is combined for the static bending analysis of FG plates. A novel shape function is developed for RPT formulation, which further improves the adaptability of RPT. Compared with HSDTs, RPT reduces one variable to improve computational efficiency. IGA solves the C1-continuity requirement problem of RPT in traditional FEA. By using T-splines based IGA, the computational efficiency is enhanced effectively. The analysis of the square plate and prismatic plate models shows the accuracy and efficiency of the method. Based on the numerical results, the thickness-to-width ratios show a negative effect on the non-dimensional deflection of FG plates while the material indexes have a positive effect. The axial stress on the bottom (metal) surface is smaller than that on the top (ceramic) surface of plate. Material indexes will affect the stress distribution patterns of the plate.

Acknowledgment

This work was supported in part by the National Natural Science Foundation of China under Grant 51935009 and U1608256, and in part by the Natural Science Foundation of Zhejiang Province under Grant Y19E050078.

References:

[1] S. Yin, T. Yu, Q.B. Tinh, X. Zheng, S. Tanaka,"In-plane material inhomogeneity of functionally graded plates: A higher-order shear deformation plate isogeometric analysis," *Compos Part B-Eng*., vol. 106, pp. 273-284, 2016.

[2] R.D. Mindlin,"Influence of rotatory inertia and shear on flexural motions of isotropic, elastic plates," *J Appl Mech-T Asme*., vol. 18, pp. 31-38, 1951.

[3] M. Bodaghi, M. Shakeri, M.M. Aghdam,"Thermo-mechanical behavior of shape adaptive composite plates with surface-bonded shape memory alloy ribbons," *Compos Struct*., vol. 119, pp. 115-133, 2015.

[4] J.N. Reddy,"Analysis of functionally graded plates," *Int J Numer Meth Eng*., vol. 47, pp. 663-684, 2000.

[5] J.N. Reddy,"A simple higher-order theory for laminated composite plates," *J Appl Mech-T Asme*., vol. 51, pp. 745-752, 1984.

[6] M. Levinson,"An accurate, simple theory of the statics and dynamics of elastic plates," *Mech Res Commun*., vol. 7, pp. 343-350, 1980.

[7] H. Nguyen-Xuan, C.H. Thai, T. Nguyen-Thoi,"Isogeometric finite element analysis of composite sandwich plates using a higher order shear deformation theory," *Compos Part B-Eng*., vol. 55, pp. 558-574, 2013.

[8] K.P. Soldatos,"A transverse-shear deformation-theory for homogeneous monoclinic plates," *Acta Mech*., vol. 94, pp. 195-220, 1992.

[9] N. Grover, D.K. Maiti, B.N. Singh,"A new inverse hyperbolic shear deformation theory for static and buckling analysis of laminated composite and sandwich plates," *Compos Struct*., vol. 95, pp. 667-675, 2013.

[10] Z. Liu, C. Wang, G. Duan, J. Tan,"A new refined plate theory with isogeometric approach for the static and buckling analysis of functionally graded plates," *Int J Mech Sci*., vol. 161, pp. 2019.

[11] M. Karama, K.S. Afaq, S. Mistou,"Mechanical behaviour of laminated composite beam by the new multi-layered laminated composite structures model with transverse shear stress continuity," *Int J Solids Struct*., vol. 40, pp. 1525-1546, 2003.

[12] M. Karama, K.S. Afaq, S. Mistou,"A new theory for laminated composite plates," *P I Mech Eng L-J Mat*., vol. 223, pp. 53-62, 2009.

[13] M. Aydogdu,"A new shear deformation theory for laminated composite plates," *Compos Struct*., vol. 89, pp. 94-101, 2009.

[14] A. Farzam, B. Hassani,"A new efficient shear deformation theory for FG plates with in-plane and through-thickness stiffness variations using isogeometric approach," *Mech Adv Mater Struc*., vol. 26, pp. 512-525, 2019.

[15] R. Sahoo, B.N. Singh,"A new shear deformation theory for the static analysis of laminated composite and sandwich plates," *Int J Mech Sci*., vol. 75, pp. 324-336, 2013.

[16] C.H. Thai, A.J.M. Ferreira, S.P.A. Bordas, T. Rabczuk, H. Nguyen-Xuan,"Isogeometric analysis of laminated composite and sandwich plates using a new inverse trigonometric shear deformation theory," *Eur J Mech A-Solid*., vol. 43, pp. 89-108, 2014.

[17] N.R. Senthilnathan, S.P. Lim, K.H. Lee, S.T. Chow,"Buckling of shear-deformable plates," *Aiaa J*., vol. 25, pp. 1268-1271, 1987.

[18] R.P. Shimpi,"Refined plate theory and its variants," *Aiaa J*., vol. 40, pp. 137-146, 2002.

[19] R.P. Shimpi, H.G. Patel,"A two variable refined plate theory for orthotropic plate analysis," *Int J Solids Struct*., vol. 43, pp. 6783-6799, 2006.

[20] R.P. Shimpi, H.G. Patel,"Free vibrations of plate using two variable refined plate theory," *J Sound Vib*., vol. 296, pp. 979-999, 2006.

[21] S. Brischetto, E. Carrera,"Advanced mixed theories for bending analysis of functionally graded plates," *Comput Struct*., vol. 88, pp. 1474-1483, 2010.

[22] L.V. Tran, T. Nguyen-Thoi, C.H. Thai, H. Nguyen-Xuan,"An Edge-Based smoothed discrete shear gap method using the C-0-Type Higher-Order shear deformation theory for analysis of laminated composite plates," *Mech Adv Mater Struc*., vol. 22, pp. 248-268, 2015.

[23] C.H. Thai, L.V. Tran, D.T. Tran, T. Nguyen-Thoi, H. Nguyen-Xuan,"Analysis of laminated composite plates using higher-order shear deformation plate theory and node-based smoothed discrete shear gap method," *Appl Math Model*., vol. 36, pp. 5657-5677, 2012.

[24] H. Thai, D. Choi,"Finite element formulation of various four unknown shear deformation theories for functionally graded plates," *Finite Elem Anal Des*., vol. 75, pp. 50-61, 2013.

[25] T. Hughes, J.A. Cottrell, Y. Bazilevs,"Isogeometric analysis: CAD, finite elements, NURBS, exact geometry and mesh refinement," *Comput Method Appl M*., vol. 194, pp. 4135-4195, 2005.

[26] G. Zhang, R. Alberdi, K. Khandelwal,"Analysis of three-dimensional curved beams using isogeometric approach," *Eng Struct*., vol. 117, pp. 560-574, 2016.

[27] A. Borkovic, S. Kovacevic, G. Radenkovic, S. Milovanovic, D. Majstorovic,"Rotation-free isogeometric dynamic analysis of an arbitrarily curved plane Bernoulli-Euler beam," *Eng Struct*., vol. 181, pp. 192-215, 2019.

[28] T. Hageman, K.M.P. Fathima, R. de Borst,"Isogeometric analysis of fracture propagation in saturated porous media due to a pressurised non-Newtonian fluid," *Comput Geotech*., vol. 112, pp. 272-283, 2019.

[29] S. Nishi, K. Terada, I. Temizer,"Isogeometric analysis for numerical plate testing of dry woven fabrics involving frictional contact at meso-scale," *Comput Mech*., vol. 64, pp. 211-229, 2019.

[30] A. Gupta, A. Ghosh,"Static and transient analysis of sandwich composite plates using isogeometric analysis," *Mech Adv Mater Struc*., vol. 26, pp. 81-87, 2019.

[31] C.H. Thai, H. Nguyen-Xuan, S.P.A. Bordas, N. Nguyen-Thanh, T. Rabczuk,"Isogeometric

analysis of laminated composite plates using the Higher-Order shear deformation theory," *Mech Adv Mater Struc*., vol. 22, pp. 451-469, 2015.

[32] C.H. Thai, A.J.M. Ferreira, T.D. Tran, P. Phung-Van,"Free vibration, buckling and bending analyses of multilayer functionally graded graphene nanoplatelets reinforced composite plates using the NURBS formulation," *Compos Struct*., vol. 220, pp. 749-759, 2019.

[33] M. Arefi, E.M. Bidgoli, A.M. Zenkour,"Free vibration analysis of a sandwich nano-plate including FG core and piezoelectric face-sheets by considering neutral surface," *Mech Adv Mater Struc*., vol. 26, pp. 741-752, 2019.

[34] Q.X. Lieu, D. Lee, J. Kang, J. Lee,"NURBS-based modeling and analysis for free vibration and buckling problems of in-plane bi-directional functionally graded plates," *Mech Adv Mater Struc*., vol. 26, pp. 1064-1080, 2019.

[35] L.C. Trinh, T.P. Vo, T. Huu-Tai, N. Trung-Kien, P. Keerthan,"State-space Levy solution for size-dependent static, free vibration and buckling behaviours of functionally graded sandwich plates," *Compos Part B-Eng*., vol. 149, pp. 144-164, 2018.

[36] D. Duc Hong, V.D. Thom, M.P. Phuc, D.D. Nguyen,"Validation simulation for free vibration and buckling of cracked Mindlin plates using phase-field method," *Mech Adv Mater Struc*., vol. 26, pp. 1018-1027, 2019.

[37] T. Yu, S. Yin, Q.B. Tinh, C. Liu, N. Wattanasakulpong,"Buckling isogeometric analysis of functionally graded plates under combined thermal and mechanical loads," *Compos Struct*., vol. 162, pp. 54-69, 2017.

[38] Y. Bazilevs, V.M. Calo, J.A. Cottrell et al,"Isogeometric analysis using T-splines," *Comput Method Appl M*., vol. 199, pp. 229-263, 2010.

[39] X. Li, J. Zheng, T.W. Sederberg, T.J.R. Hughes, M.A. Scott,"On linear independence of T-spline blending functions," *Comput Aided Geom D*., vol. 29, pp. 63-76, 2012.

[40] M.A. Scott, X. Li, T.W. Sederberg, T.J.R. Hughes,"Local refinement of analysis-suitable T-splines," *Comput Method Appl M*., vol. 213-216, pp. 206-222, 2012.

[41] L.B. Da Veiga, A. Buffa, G. Sangalli, R. Vazquez,"Analysis-suitable t-splines of arbitrary degree: Definition, linear independence and approximation properties," *Math Mod Meth Appl S*., vol. 23, pp. 1979-2003, 2013.

[42] H. Thai, S. Kim,"A size-dependent functionally graded Reddy plate model based on a modified couple stress theory," *Compos Part B-Eng*., vol. 45, pp. 1636-1645, 2013.

[43] L.V. Tran, P. Phung-Van, J. Lee, M.A. Wahab, H. Nguyen-Xuan,"Isogeometric analysis for nonlinear thermomechanical stability of functionally graded plates," *Compos Struct*., vol. 140, pp. 655-667, 2016.

[44] Q.B. Tinh, V.D. Thom, H.T.T. Lan et al,"On the high temperature mechanical behaviors analysis of heated functionally graded plates using FEM and a new third-order shear deformation plate theory," *Compos Part B-Eng*., vol. 92, pp. 218-241, 2016.

[45] T. Mori, K. Tanaka,"Average stress in matrix and average elastic energy of materials with misfitting inclusions," *ACTA METALLURGICA*., vol. 21, pp. 571-574, 1973.

[46] T.N. Sederberg, J.M. Zheng, A. Bakenov, A. Nasri,"T-splines and T-NURCCs," *Acm T Graphic*., vol. 22, pp. 477-484, 2003.

[47] R. Dimitri, L. De Lorenzis, M.A. Scott et al,"Isogeometric large deformation frictionless contact

using T-splines," *Comput Method Appl M.*, vol. 269, pp. 394-414, 2014.

[48] D.C. Thomas, M.A. Scott. "Isogeometric analysis based on T-splines," 2015;561:205-232

[49] S.H. Habib, I. Belaidi,"Extended isogeometric analysis using analysis-suitable T-splines for plane crack problems," *Mechanika.*, vol. 23, pp. 11-17, 2017.

[50] T. Uhm, S. Youn,"T-spline finite element method for the analysis of shell structures," *Int J Numer Meth Eng.*, vol. 80, pp. 507-536, 2009.

[51] J.S. Hale, P.M. Baiz,"A locking-free meshfree method for the simulation of shear-deformable plates based on a mixed variational formulation," *Comput Method Appl M.*, vol. 241, pp. 311-322, 2012.

[52] J. Kiendl, K. Bletzinger, J. Linhard, R. Wuechner,"Isogeometric shell analysis with Kirchhoff-Love elements," *Comput Method Appl M.*, vol. 198, pp. 3902-3914, 2009.

[53] D. Wang, J. Xuan,"An improved NURBS-based isogeometric analysis with enhanced treatment of essential boundary conditions," *Comput Method Appl M.*, vol. 199, pp. 2425-2436, 2010.

[54] F. Auricchio, L.B. Da Veiga, A. Buffa et al,"A fully "locking-free" isogeometric approach for plane linear elasticity problems: A stream function formulation," *Comput Method Appl M.*, vol. 197, pp. 160-172, 2007.